


Article

The Impact of Climate Change on Evapotranspiration and Flow in a Major Basin in Northern Mexico

Aldo Rafael Martínez-Sifuentes ¹, Ramón Trucíos-Caciano ¹, Víctor Manuel Rodríguez-Moreno ², José Villanueva-Díaz ¹ and Juan Estrada-Ávalos ^{1,*}

¹ Instituto Nacional de Investigaciones Forestales, Agrícolas y Pecuarias, CENID-RASPA, Gómez Palacio C.P. 35150, Durango, Mexico

² Instituto Nacional de Investigaciones Forestales, Agrícolas y Pecuarias, Campo Experimental Pabellón, Km 32.5, Carretera Aguascalientes—Zacatecas, Pabellón de Arteaga C.P. 20660, Aguascalientes, Mexico

* Correspondence: estrada.juan@inifap.gob.mx

Abstract: Climate defines the hydrological cycle of each region and climate change will undoubtedly affect the recharge processes of the world's water tables and the water resources currently available at the basin and microbasin scale. The objective of the present paper is to evaluate future changes in evapotranspiration and flows from the Sardinias River basin in North Durango, Mexico. The Rural Genius Model (GR2M) is an aggregated monthly hydrological model, which is used to reconstruct flows from precipitation and evapotranspiration by applying two functions: a production function and a transfer function. A transfer function has been used under four shared socioeconomic pathway scenarios (126, 245, 370, and 585). Pettitt and Mann–Kendall statistical tests were used to determine trends, which were identified by the breakpoint in the evapotranspiration and flow time series. Results showed that under climate change scenarios, evapotranspiration shows an increase over time. Under the climate scenario, SSP 126, and the application of the statistical test in the flow series show an increasing trend with a break in May for 2090, with a mean of 1658 mm before and 2238 mm after the break, with an excess of 34.98%. The flow under the SSP 245 climate scenario predicts a mean flow of 1703.11 mm and a break in May of the 2090 horizon, with a mean before and after the break of 1624 mm and 2168 mm, respectively, with an excess of 33.49%. Under the SSP 370 scenario, the mean is expected to be 1710.81 mm, with a break in May 2090, before and after means of 1633 mm and 2166 mm, respectively, with an excess of 32.63%. Under climate change scenario SSP 585, the mean expected will be 1701.43 mm and the break in the flow series will occur in May of the 2090 horizon, with a mean of 1628 mm before the break and 2132 mm after, with a flow excess of 30.95%. The results of this study can be a basis for decision-makers for better management and protection of water resources in northern Durango, Mexico.

Keywords: climate change; evapotranspiration; flow; Sardinias River basin; trend



Citation: Martínez-Sifuentes, A.R.; Trucíos-Caciano, R.; Rodríguez-Moreno, V.M.; Villanueva-Díaz, J.; Estrada-Ávalos, J. The Impact of Climate Change on Evapotranspiration and Flow in a Major Basin in Northern Mexico. *Sustainability* **2023**, *15*, 847. <https://doi.org/10.3390/su15010847>

Academic Editor: Yong Xiao

Received: 29 September 2022

Revised: 13 December 2022

Accepted: 26 December 2022

Published: 3 January 2023



Copyright: © 2023 by the authors. Licensee MDPI, Basel, Switzerland. This article is an open access article distributed under the terms and conditions of the Creative Commons Attribution (CC BY) license (<https://creativecommons.org/licenses/by/4.0/>).

1. Introduction

Access to water has dramatically decreased for a large number of both human and wildlife populations due to overexploitation and mismanagement of the resource, especially in areas where water for agriculture and industry present the greatest challenges [1]. With the growing problem of water shortages and declining water quality, the impact on societies as a whole is notorious and events such as floods, droughts, and groundwater contamination have been compounded by global warming [2,3].

The period of insolation and the frequency and intensity of rainfall events in the Sierra Madre Occidental (SMO) physiographic province (located in the northwestern region of northern Mexico) are influenced by global climatic phenomena, such as the El Niño Southern Oscillation, and continental phenomena, such as the Pacific Decadal Oscillation and the North American Monsoon System. These phenomena cause significant annual

precipitation (450–1500 mm) over the mountain range [4] and the North American Monsoon System by itself contributes approximately 70% of the total annual precipitation recorded in this region [5]. Although this climate system has significant effects in its area of influence (i.e., the southern United States and northern Mexico), its greatest activity is centered in the SMO, where most of the convective systems are formed and the greatest amount of precipitation falls [6].

This condition allowed the development of large irrigation districts on both slopes of the SMO, supplied by a large number of dams that were promoted by the agricultural policy of Mexico since the middle of the 20th century. Most of the runoff associated with monsoon rains occurs on the eastern slope of the SMO, where the Sextín River basin (SRB) and Irrigation District 017 are located.

Climate defines the hydrological cycle of each particular region on Earth and there is no doubt that climate change will affect the world's water table recharge processes and the currently available water resources at the basin and micro-basin scale [7]. In Mexico, the impacts of climate change on the water cycle will be reflected by a decrease in the volume of surface water, and the level and quality of groundwater.

These impacts will be more evident in those regions where there is a greater demand for water resources (surface and groundwater) and in overexploited aquifers [8]. Given this situation, it is important to establish the impact that climate change will have on the variables and factors that define the hydrological cycle, and to develop strategies for the management of water resources. Therefore, knowledge of the functioning of the resource in water-producing basins is required.

In recent decades, several hydrological models have been proposed that address the rainfall–flow relationship along with improvements in flexibility and database management. Among these is the Rural Genius model developed by the French Research Institute for Agricultural and Environmental Engineering. Rural Genius is a test ecosystem that works with different database intervals (e.g., annual [GR1A], monthly [GR2M], and daily [GR4J]). This hydrological model has been widely used by several authors with satisfactory results [1,9,10]. In a study by Segura-Méndez [11], the GR2M model showed the best fit in semi-arid and sub-humid basins (the predominant climate of the Sextín River basin), with a correlation coefficient close to 0.90 compared to the monthly water balance simulation models Témez, ABCD, GUO5P, and Thornthwaite–Mather. The better performance of the GR2M model compared to the SWAT model has also been found, with Nash and R^2 values of up to 0.66 [12]. A rainfall model is important to forecast the availability of the resource, and in conjunction with climate scenarios, the resource's future availability.

Global climate models have been the primary tool for examining past and future climate. Recently, a new generation of global climate models has been developed in the operational framework of the Coupled Model Intercomparison Project Phase 6 (CMIP6 project) [13]. The key to the success of CMIP6 in representing simulations (e.g., the carbon cycle) is that it reduces duplication of effort, minimizes operational and computational burden, and delineates common practices in the generation and analysis of the resulting large databases [13]. The newer global climate models have an increased degree of complexity in physical processes and higher spatial resolution.

CMIP6 climate models are mostly used to assess changes in climate for past or future periods to obtain a more detailed understanding of the physical aspects and processes of climate change [14]. In the face of new and improved global climate models, some climate change scenarios (i.e., Shared Socioeconomic Pathways [SSPs]) have been calculated [15]. Along with a set of mitigations (e.g., the development of society, the regulatory framework, migration to urban centers, economic activities, and the sustainable use of natural capital), these SSPs will allow researchers and governments to examine how possible catastrophic scenarios can be avoided in the future.

Considering the above, the objective of this study was to evaluate the evapotranspiration trend and flow behavior for the 2030, 2050, 2070, and 2090 climate horizons under the

SSP 126, 245, 370, and 585 scenarios with the GR2M monthly aggregated model and the Coupled Model Intercomparison Projects-6 Global Circulation Model CNRM-CM6-1.

2. Materials and Methods

2.1. Study Area

The SRB is located in the upper part of the Nazas River basin, north of hydrologic region No. 36, at extreme coordinates $25^{\circ}34' - 26^{\circ}30' N$ and $104^{\circ}57' - 106^{\circ}20' W$ in the state of Durango, Mexico (Figure 1). The SRB originates in the SMO to the east of the Balleza and Colorado River basins, to the south of the Sierra del Oso, and to the northwest of the Sierra la Candela. The surface area of the watershed is 4805 km^2 , with an elevation gradient from 1623 to 3164 masl [16]. Five types of climate prevail in the SRB: temperate sub-humid, semi-cold, temperate, semi-dry temperate, and semi-dry warm [17]. The average annual precipitation is 608 mm, the monthly mean minimum temperature is $6.42 \text{ }^{\circ}\text{C}$, and the monthly mean maximum temperature is $24.98 \text{ }^{\circ}\text{C}$ [18]. Historically, the tendency of precipitation in the Sextín River basin has been decreasing, with minimum annual accumulated values from 366 mm to 906 mm, a situation similar to that of runoff with flows of $924 \text{ m}^3 \text{ s}^{-1}$ to $2757 \text{ m}^3 \text{ s}^{-1}$, with a tendency to decrease in recent years. The geological, geophysical, and hydrogeological evidence allows us to define the presence of a heterogeneous and anisotropic free type aquifer, constituted in its upper portion, by alluvial sediments of varied granulometry and conglomerates, whose thickness can reach several meters in the center of the valley. The hydraulic parameters establish that the aquifer has a transmissivity of 1.82×10^{-2} and $4.36 \times 10 \text{ m}^2 \text{ s}^{-1}$, with an average value of $8.28 \times 10^{-3} \text{ m}^2 \text{ s}^{-1}$, and the conductivity values vary from 1.42×10^{-4} and $1.76 \times 10^{-5} \text{ m s}^{-1}$, with an average value of $6.46 \times 10^{-5} \text{ m s}^{-1}$ for the recovery stage.

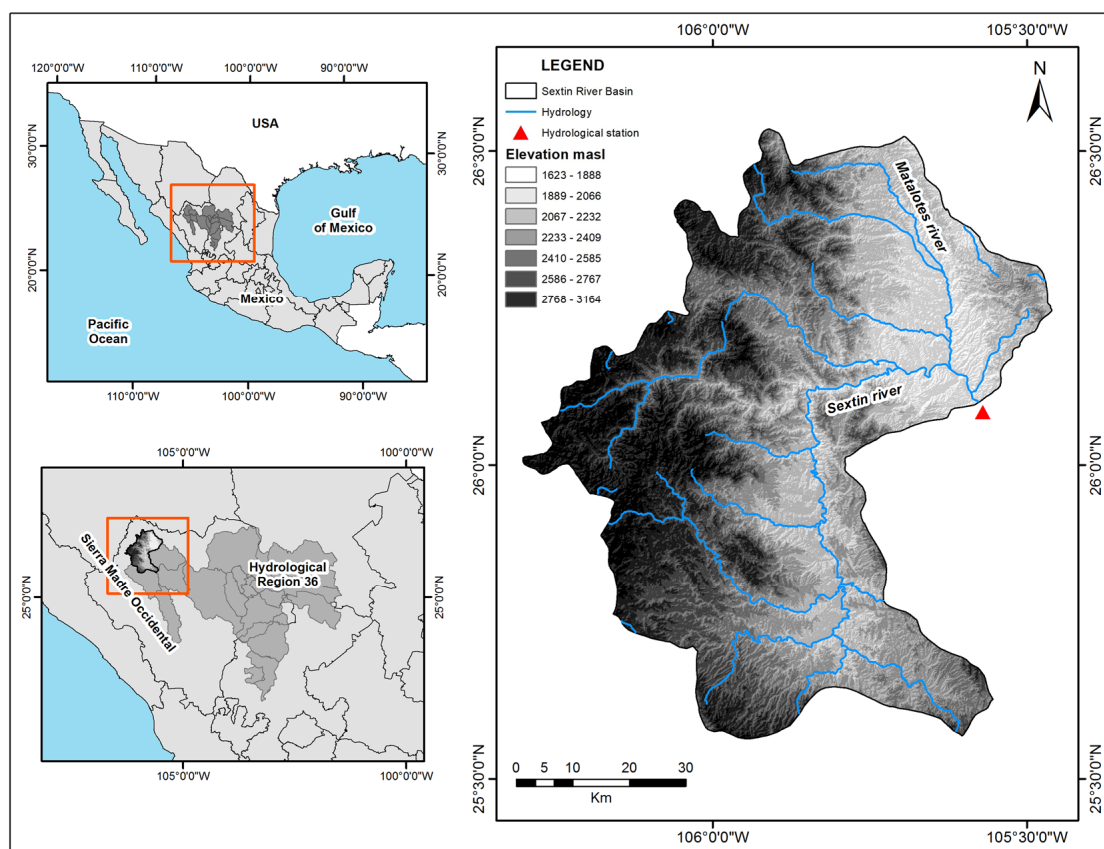


Figure 1. The location of the Sextín River basin in the state of Durango, Mexico.

2.2. The GR2M Model and Hydro-Environmental Variables

The GR2M model was used to determine the impact of climate change on future runoff in the SRB under four climate change scenarios [i.e., Shared Socioeconomic Pathways (SSPs 126, 245, 370, and 585)] from the CNRM-CM6-1 model. SSPs describe alternative futures of socioeconomic development and represent, based on narrative and quantitative variables, how the world might evolve in the coming decades and what challenges these changes pose for mitigation and adaptation. The SSP1 scenario combines low levels of mitigation and adaptation challenges, SSP3 assumes high population growth and low economic development, and SSP2 scenarios are set intermediate between those corresponding to SSP1 and SSP3. The SSP5 narrative maintains low population growth, this scenario assumes that this low population growth also includes rapid technological change, coupled with intensive use of fossil fuels. This scenario maintains high mitigation challenges, as the levels and type of energy assumed lead to a world of high emissions and a subsequent increase of about 5 degrees Celsius in temperature by 2100. The CNRM-CM6-1 model generates a better representation of the climate system in terms of the average state and variability. It was released in 2017 and includes the aerosol, atmos, Gaussian diminished, 91 levels, atmosChem, Surfex, Nemo, and Sea ice components. The scenarios were downloaded from the WorldClim interface (https://www.worldclim.org/data/cmip6/cmip6_clim2.5m.html accessed on 25 January 2021).

The downloaded images are in GeoTiff format and include the following variables: maximum average temperature ($^{\circ}\text{C}$), minimum average temperature ($^{\circ}\text{C}$), and accumulated precipitation in the month (mm). Four SSP scenarios were evaluated for the periods 2021–2040 (2030 horizon), 2041–2060 (2050 horizon), 2061–2080 (2070 horizon), and 2081–2100 (2090 horizon), with a spatial resolution of $2.5' \times 2.5'$ ($\sim 19.87 \text{ km}^2$) [19]. The GR2M monthly model was developed in France by Makhlof and Michel [20] and is useful in arid and semi-arid areas [10,21]. It allows the reconstruction of historical series of streamflows from the rainfall and evapotranspiration data.

The model (Figure 2) assumes that in each basin there are two water storage reservoirs (i.e., the production store [maximum storage capacity of the soil] and the routing store [gravitational water storage]). The soil, represented by S_i , controls for the coefficient X_1 (in mm) and the groundwater storage, represented by R_i (mm), controls for the coefficient X_2 . In all stages of the model, R_i has a reference parameter of 60 mm, which is a reservoir with a maximum capacity of 60 mm that controls the transfer function [19]. Inputs to the model are the monthly precipitation value (P) and the monthly potential evapotranspiration value (PET); the resulting product is runoff (Q) in mm (units derived from the maximum R_i capacity (mm) and evapotranspiration (mm), which translates into a water flow sheet). To correct water balance errors, the GR2M model has an additional parameter X_2 (dimensionless groundwater exchange coefficient in the basin), which allows the correction of possible biases due to historical climate and runoff conditions [20].

At each stage (red numbers) of the model, precipitation is channeled by infiltration to the production store (Stage 1), or directly to the routing reservoir through surface flow (P_1 ; Stage 2). If the reservoir reaches the S_1 level (mm), it loses part through evaporation (E) (Stage 3), until it reaches the S_2 level (mm) and becomes part of the soil moisture P_2 (mm) (the volume of the percolating water), and is then transferred to the routing reservoir by percolation through the soil (Stage 4).

The sum of P_1 and P_2 (P_3 ; Stage 5) joins the routing reservoir until it reaches the R_i level (Stage 6). There will be a loss or gain of water in the routing reservoir by the exchange between the subsurface and surrounding areas outside the basin (Stage 7). If the coefficient $X_2 > 1$, it means that there is an inflow of water from the outside to the inside of the basin, and if $X_2 < 1$, there will be an outflow (Q_i) from the routing reservoir to the surrounding basins (Stage 8). The GR2M hydrological model is subject to the premise that in the course of its stages, there may be processes of inflow or outflow of water from neighboring basins, and in such a situation, the parameters X_1 and X_2 are optimized.

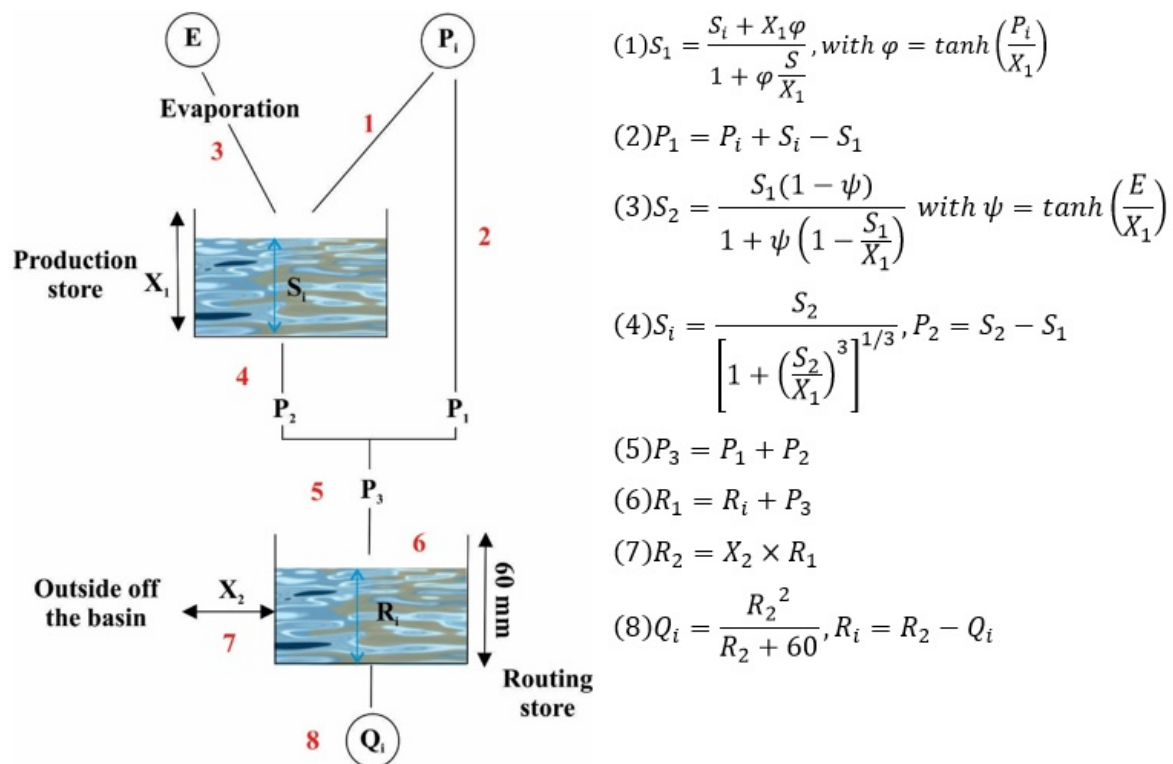


Figure 2. Structure of the GR2M model (modified by Mouelhi et al. [22]). Figure adapted and edited by the authors.

To calibrate the model, monthly-observed data from January 1970 to December 1988 were used. The first two years were used for the warm-up period and the remaining years for the calibration period. The validation of the model was developed with monthly-observed data from January 1989 to December 2006.

To evaluate the performance of the GR2M model, the Nash criterion [23], the percentage bias PBIAS, and the absolute percentage bias APBIAS [24] were used, which are based on comparing the estimated and observed flow and are represented as follows:

$$Nash = 100 \times \left[1 - \frac{\sum (Q_{obs} - Q_{est})^2}{\sum (Q_{obs} - \bar{Q}_{obs})^2} \right] \quad (1)$$

$$PBIAS = 100 \left[\frac{\sum (Q_{obs} - Q_{est})}{\sum Q_{obs}} \right] \quad (2)$$

and

$$APBIAS = 100 \left[\frac{\sum abs(Q_{obs} - Q_{est})}{\sum Q_{obs}} \right] \quad (3)$$

where Q_{obs} is the observed flow (mm), Q_{est} is the estimated flow (mm), and \bar{Q}_{obs} is the average observed flow (mm).

The performance of the GR2M model is considered sufficient when the estimated flow is close to the observed flow (i.e., when Nash is close to 100%). The model is insufficient when $Nash < 0.2$, satisfactory when $Nash = 0.2-0.4$, good when $Nash = 0.4-0.6$, very good when $Nash = 0.6-0.8$, and excellent when $Nash > 0.8$ [25]. For the PBIAS criterion, a percentage within the range from -25% to 25% is expected to classify it as correct in the calibration and validation stages. The optimal APBIAS value should be close to zero (a range of 0.0–0.5).

The observed flow (i.e., the monthly records from 1970 to 2006) information came from hydrologic station number 36,071, Sardinias ($26^{\circ}4'59.88''$ N, $105^{\circ}34'12.00''$ W). It was

downloaded from the National Surface Water Data Bank of the National Water Commission. Monthly potential evapotranspiration was estimated using the empirical model of Hargreaves and Samani [26], which is based on environmental variables, such as air temperature and extraterrestrial solar radiation. Maximum, minimum, and monthly mean air temperature and monthly mean cumulative precipitation were obtained from ClimateNA, which is based on the Climate Research Unit database (CRU TSA TS4.04), with a spatial resolution of $0.5^\circ \times 0.5^\circ$ covering the period from 1970 to 2006 [18]. The equation for estimating PET is as follows:

$$PET = \frac{0.0023(T_{mean} + 17.8)(T_{max} - T_{min})^{0.5} Ra}{\lambda} \quad (4)$$

where T_{mean} is the monthly mean temperature ($^\circ\text{C}$), T_{max} is the monthly maximum temperature ($^\circ\text{C}$), T_{min} is the monthly minimum temperature ($^\circ\text{C}$), Ra is the extraterrestrial solar radiation ($\text{MJ m}^{-2} \text{ day}^{-1}$), and λ is the monthly latent heat of vaporization (MJ Kg^{-1}). Extraterrestrial solar radiation was estimated using the tables proposed by the Food and Agriculture Organization [27] using 26.052° N of the SRB centroid.

The monthly latent heat of vaporization was calculated with the following equation and was used to directly obtain PET in mm day^{-1} :

$$\lambda = 2.501 - 0.002361 T_{mean} \quad (5)$$

Under the same criteria used for the current scenario with the observed monthly data, the parameters X_1 and X_2 were transferred to the GR2M model for the future climate horizons in the calibration and validation stages. To estimate the direction in historical trends of the flows and the PET, as well as the break dates of these series, Pettitt tests and Mann–Kendall tests were performed using R software version 3.4.3 with the Trend and Kendall libraries [28].

2.3. Pettitt's Test

The Pettitt test ($p < 0.05$) allows the examination of a breakpoint in a time series derived from a Mann–Whitney test [29] and is based on the calculation of U_t , which is defined by the following equation [30]:

$$U_{t=\sum_{i=1}^t \sum_{j=i+1}^n \text{sign}(x_t - x_j)} \quad (6)$$

where $\text{sign}(x_t - x_j) = -1$ if $(x_t - x_j) < 0$, $D_{ij} = 0$ if $(x_t - x_j) = 0$, $D_{ij} = 1$ if $(x_t - x_j) > 0$.

2.4. Mann–Kendall Test

We used the Mann–Kendall test ($p = 0.05$) to detect the presence or absence of a monotonic linear trend in a time series [31,32]. We used the series $A_i (a_1, a_2, \dots, a_n)$, where the multivariate standard U_{MK} is calculated as follows:

$$U_{MK} = \frac{S}{\sqrt{\text{Var}(s)}} \quad (7)$$

with $S = \sum_{i=1}^{n-1} \sum_{j=i+1}^n \text{sgn}(a_j - a_i)$, $\text{Var}(s) = \frac{n(n-1)(2n+5)}{18}$, where n is the number of data in the series.

The existence of a trend in the time series is defined with the UMK coefficient; if $U > 0$, the trend is upward and if $U < 0$, the trend is downward.

3. Results and Discussions

3.1. Flow and Evapotranspiration Trends

The hydrologic result of the flow time series obtained from the Sardinas station located downstream of the SRB (Figure 3), using the Mann–Kendall test, shows a downward trend, with a multivariate standard UMK of -0.032 . This trend is corroborated by the Pettitt test,

which shows a break in the series in October 1992, with a mean before and after that date of 18.84 and $10.54 \text{ m}^3 \text{ s}^{-1}$, respectively. Contributing factors in that decade (the 1990s) include an intense El Niño condition [33], as well as changes in rainfall regimes identified through the standardized precipitation index [34].

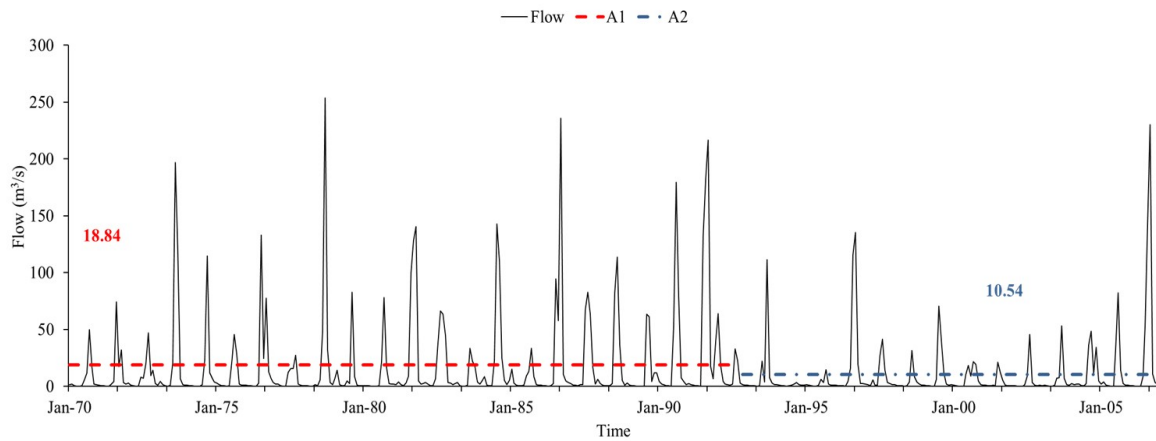


Figure 3. Historical flow at Sardinas station from 1970 to 2006. A1 = mean before the break and A2 = mean after the break.

To analyze the effects of precipitation on the flow in the SRB, a relationship between precipitation and observed flow was generated (Figure 4). The close association between precipitation and flow allowed observation of the maximum values of runoff and rainfall in periods 1–7 (Figure 4a), a situation evidenced by an R-value of 0.80 ($n = 444$, $p < 0.05$; Figure 4b). The synchrony between maximum precipitation and runoff values occurs in the summer season (July, August, and September) when the maximum flow is caused by precipitation. These years were characterized by seasonal periods with extraordinary precipitation above the monthly average that were recorded in hydrological stations in the state of Durango in the years 1973, 1976, 1978, 1981, 1986, 1987, 1993, 1996, and 2006 [35].

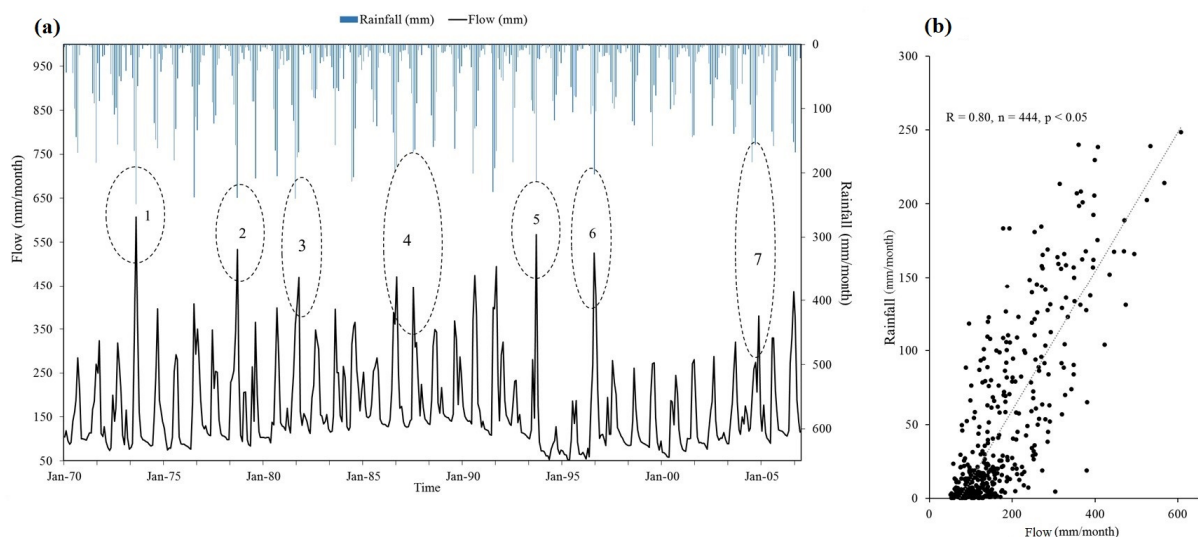


Figure 4. The relationship between precipitation and flow at the Sardinas hydrometric station. (a) The ovals with broken lines numbered from 1 to 7 represent the periods with maximum runoff and precipitation values. (b) Scatter plot between runoff and precipitation.

These coincident maximum values are attributed to the high volume of precipitation because when the volume exceeds the infiltration capacity of the soil, the soil becomes saturated when it reaches its maximum storage capacity and favors surface runoff [36].

There are also other biophysical factors that generate a strong precipitation–runoff relationship, such as vegetation density and composition, soil roughness, slope, pedregosity (the presence on the surface of large fragments from 7.5 to 25 cm in diameter) of soil, and soil type, all of which influence the rate of water infiltration into the soil profile [37].

Outside of these coincident periods, the flow recorded at the Sardinias hydrometric station shows decreases and increases, where the average historical flow was 170.79 mm. The maximum flow recorded in July 1973 was 607 mm and the precipitation was 248.5 mm, which coincided with the North American Monsoon System, a climatic phenomenon that provides 70% of the annual precipitation in northern Mexico [38–40]. A minimum flow of 51 mm occurred in May 1995 and precipitation was 2.5 mm, a period that is known as the pre-monsoon season [5].

The potential evapotranspiration estimated by Hargreaves and Samani [24], with temperature data from re-analysis of the period 1970–2006, presented a historical mean of 134.00 mm, with a maximum PET of 209.38 mm for May 1989 and a minimum PET of 65.37 mm for December 1976. The Mann–Kendall analysis shows an upward trend over the 37 years of estimated PET with a slope of 0.02 mm/year, a trend corroborated by the Pettitt test, which shows a break in the series in February 1992, with a mean before and after that date of 131.86 and 137.20 mm, respectively (Figure 5), representing an increase of 4.04%.

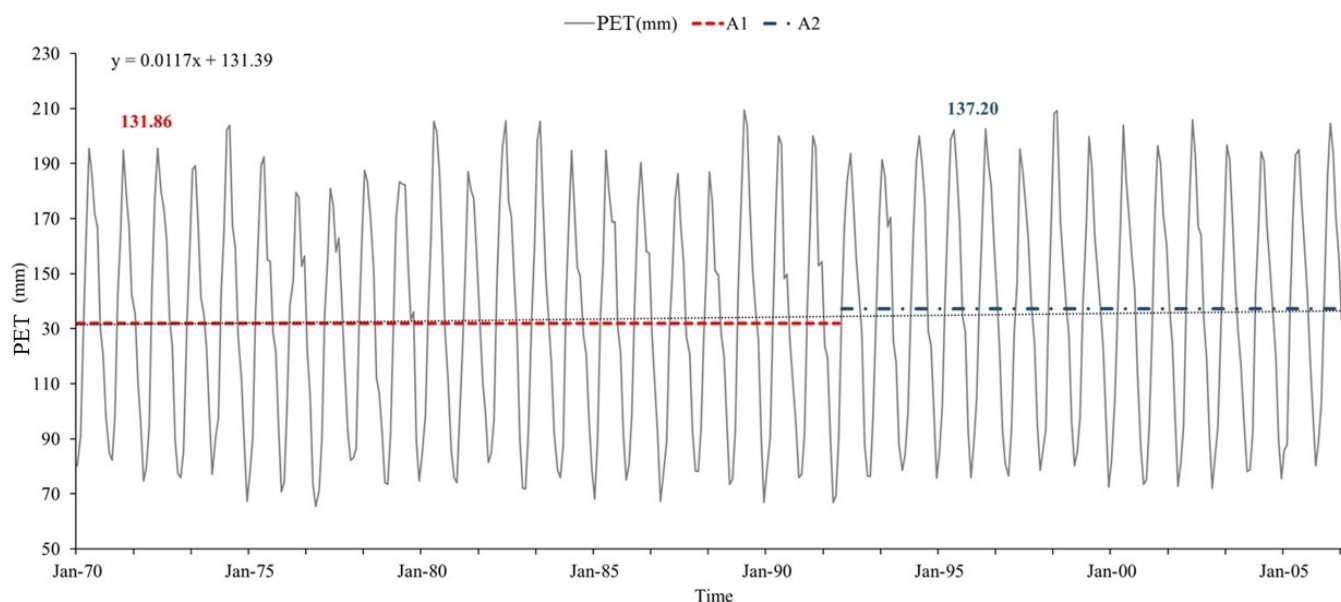


Figure 5. Historical PET for the Sextín River basin for 1970–2006 using the Pettitt test. A1 = mean before the break and A2 = mean after the break.

This increased PET was due to the trend of increasing temperatures in northern Mexico, a condition that continues to exist in the SMO; it is a region with high climate variability and historical increases in temperatures [41]. Different ocean–atmosphere phenomena impact this region. For example, La Niña, which causes periods of severe droughts due to low precipitation and high temperatures [42] and results in changes in the parameters of the hydrological cycle, such as the PET [43]. A large number of studies have explained the mechanisms behind the change in the PET trend from the perspective of climatic conditions and the properties of the earth’s surface [44–46]. Studies suggest that changes in climatic conditions (e.g., warming, wind quenching, and changes in precipitation and relative humidity/vapor pressure deficit) drive PET variations in some regions by regulating water and energy conditions. In contrast, in other regions, land surface property factors predominated [45,47]. In addition, afforestation and deforestation are believed to have the functions of increasing and decreasing PET, respectively [48]. Some studies found that

forestation could reduce water yield or runoff, generally through increased evaporation of canopy interception, transpiration, and the PET [47].

3.2. Performance of the GR2M Model

The GR2M model used in the analysis is based on the Nash criteria, PBIAS, and APBIAS and is used to evaluate the performance in the calibration and validation stages, as well as the coefficient of determination R^2 . Although the GR2M model only uses two input parameters, it has been shown to perform well compared to other similar hydrological models on a monthly scale [22]. When the model performance exhibits good calibration and validation characteristics, the parameters can be applied for series under climate change, as demonstrated by Okkan and Fistikoglu [49].

For the calibration process, the parameters X_1 and X_2 were adjusted to obtain the optimum Nash value and the coefficient of determination. For the present analysis, these values were 17.17 and 0.53, respectively, with Nash = 0.78, PBIAS = 0.36%, APBIAS = 21.93%, and $R^2 = 0.72$, using monthly records from January 1970 to December 1988. For validation purposes, the data used were from January 1989 to December 2006. This resulted in Nash = 0.75, PBIAS = 2.93%, APBIAS = 23.26%, and $R^2 = 0.68$, with parameters X_1 and X_2 of 15.84 and 1.20, respectively.

Hydrographs obtained during the calibration (Figure 6a) and validation (Figure 6b) processes of the GR2M model for the SRB show Nash and R^2 evaluation criteria that classify the model as very good [25].

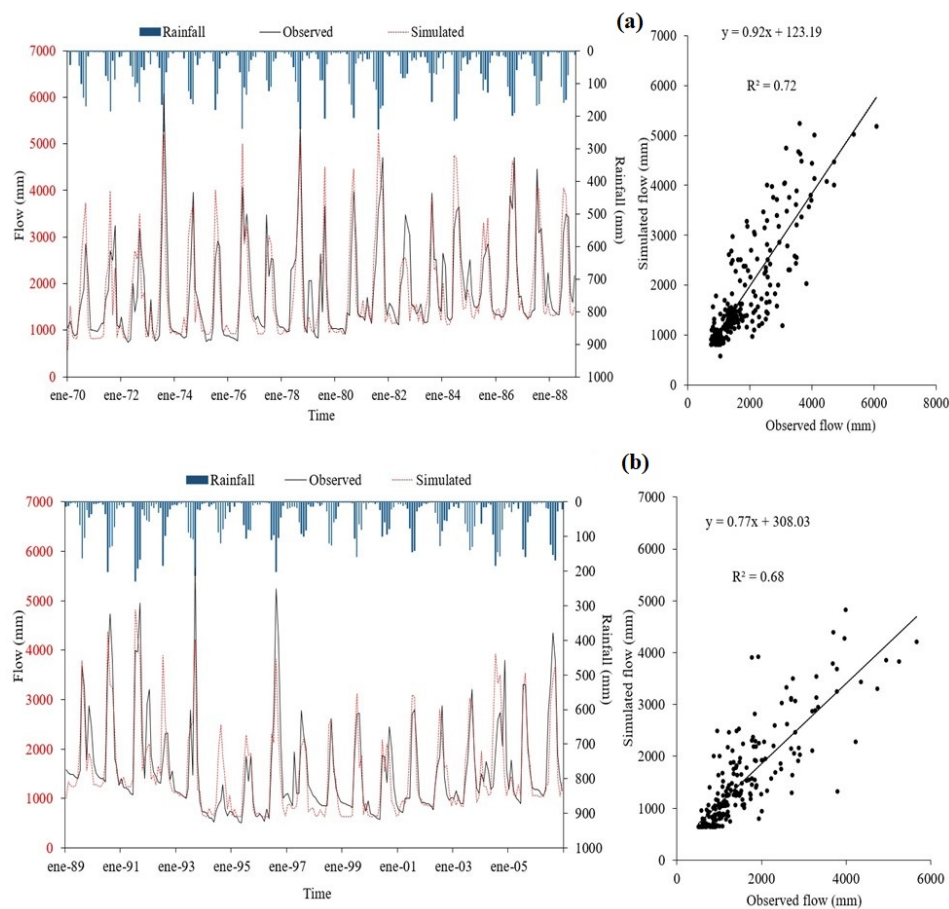


Figure 6. Calibration (a) and validation (b) of the GR2M model for the Sextín River basin. Hydrograph of observed–simulated flow and precipitation (left). Scatter plot between observed and simulated flow (right). Note: y-axes are at different scales.

3.3. Evapotranspiration and Future Flow

According to Voltaire [19], the CNRM-CM6-1 model has applications for the northern region of Mexico because of its consistent simulated behavior for the North American monsoon region [50], where much of the annual precipitation is recorded for July and August [51]. Using the Mann–Kendall and Pettitt analysis, an increase of 0.40 °C in mean annual temperature is predicted for the SSP 126 scenario, 0.36 °C, 0.33 °C, and 0.48 °C for SSP scenarios 245, 370, and 585, respectively, for the 2030 climate horizon [19], as shown in Table 1.

Table 1. Increases in mean annual temperature for climate change projections under SSP scenarios 126, 245, 370, and 585 for the SRB.

Climate Horizon	SSP 126	SSP 245	SSP 370	SSP 585
2030	0.40 °C	0.36 °C	0.33 °C	0.48 °C
2050	0.82 °C	1.17 °C	1.17 °C	1.62 °C
2070	0.99 °C	1.80 °C	2.43 °C	3.42 °C
2090	1.05 °C	2.32 °C	3.80 °C	5.59 °C

For precipitation, an increase is shown for the SSP 126 scenario of 7.52%, 4.53%, 4.39%, and 5.88% for SSP scenarios 245, 370, and 585, respectively, for the 2030 climate horizon (Table 2). This trend of increasing annual precipitation is highly variable geographically, but there have been increases during the present century between 5% and 10% in the middle and high latitudes of the northern hemisphere. The region where the SRB is located and the evidence of this variability in precipitation are according to projections of the Intergovernmental Panel on Climate Change [52].

Table 2. Variations in annual precipitation for climate change projections under SSP scenarios 126, 245, 370, and 585 for the Sextín River basin.

Climate Horizon	SSP 126	SSP 245	SSP 370	SSP 585
2030	7.52%	4.53%	4.39%	5.88%
2050	6.64%	−0.24%	6.09%	4.42%
2070	3.86%	−0.58%	−1.88%	−2.86%
2090	6.52%	0.90%	−0.08%	−3.57%

These changes in rainfall patterns are due to changes in continental and sea surface temperatures together with variations in wind patterns and ocean currents [53]. Variability was consistent with other research, which has predicted increases in precipitation for the North American monsoon zone of influence [54,55], and in the Asian monsoon region [56].

Under SSP climate scenarios 126, 245, 370, and 585, and the application of the Mann–Kendall statistical test on the future evapotranspiration series, an upward trend was shown with a slope equal to 0.00, 0.05, 0.06, and 0.09 mm/year, respectively. This trend is corroborated by the Pettitt test (Figure 7), which shows a break in the forward PET series in February 2070 for all four climate change scenarios in the study period (2021–2100). The mean monthly PET before and after the break date under the SSP 126 scenario was 132.131 mm and 142.236 mm, respectively, with an excess of 7.64%. For SSP 245, the mean before and after the break was 131.148 mm and 147.055 mm, respectively, with an excess of 12.12%; for SSP 370, it was 131.141 mm and 151.981 mm, respectively, with an excess of 14.15%; and for SSP 585, it was 134.472 mm and 158.407 mm, respectively, with an excess in PET of 17.79% (Figure 7).

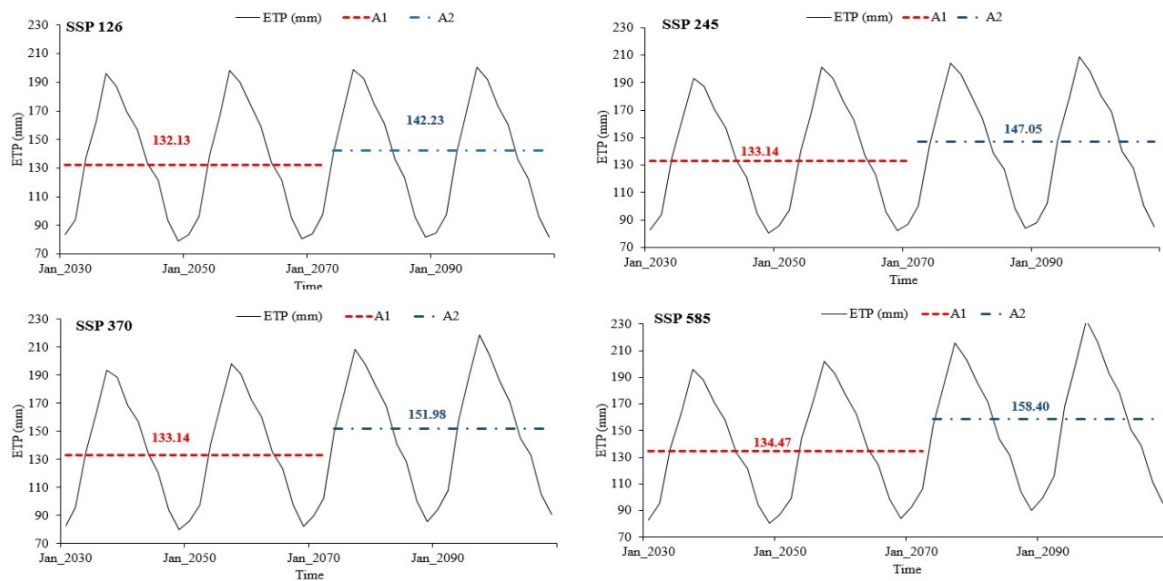


Figure 7. PET variation for SSP scenarios 126, 245, 370, and 585 over the period 2021–2100. A1 = mean before the break and A2 = mean after the break.

As PET is related to air temperature, the changes that are expected in the future (increases or decreases in PET), will be due to changes in temperature under climate change conditions [57], as well as drought trends [58] or variability in the internal climate [59].

Under the climate scenario SSP 126, a mean future flow of 1742.98 mm is predicted and the application of the Mann–Kendall test in the flow series shows an increasing trend, which is corroborated by the Pettitt test. This trend shows a break in May for the 2090 climate horizon, with a mean of 1658 mm before and 2238 mm after the break, with an excess of 34.98% (Figure 8a). The flow under the SSP 245 climate scenario predicts a mean flow of 1703.11 mm and a break in May of the 2090 horizon, with a mean before and after the break of 1624 mm and 2168 mm, respectively, with an excess of 33.49% (Figure 8b).

Under the SSP 370 scenario, the mean is expected to be 1710.81 mm, with a break in May 2090 and before and after means of 1633 mm and 2166 mm, respectively, with an excess of 32.63% (Figure 8c). Finally, under climate change scenario SSP 585, the expected mean will be 1701.43 mm, the break in the flow series will occur in May of the 2090 horizon with a mean of 1628 mm before the break and 2132 mm after, with a flow excess of 30.95% (Figure 8d).

The observed average historical flow compared to the 2030, 2050, 2070, and 2090 horizons under the SSP 126 climate scenario is expected to have an upward trend with values of 2.70%, 2.39%, 0.84%, and 2.22%, respectively (Figure 9a). For SSP 245, percentages of 1.30%, −0.94%, −1.10%, and −0.41% are expected for the horizons analyzed (Figure 9b).

The SSP 370 scenario will present percentages of 1.24%, 2.02%, −1.72%, and −0.88%, respectively, for each climate horizon (Figure 9c). Finally, the SSP 585 scenario foresees increases and decreases compared to the observed average historical flow of 1.93%, 1.24%, −2.17%, and −2.53% for each of the climate horizons (Figure 9d). Given the climate change conditions for the SRB region, the downward trend in water resources under a very adverse scenario, such as SSP 585, compared to SSP 126, is of concern. The above results are similar to those reported in other regions but with the extreme scenarios of CMIP6 245 and 585 [60]. Precipitation is the main source of runoff replenishment in the SRB, so runoff is affected by the difference in the seasonal distribution of precipitation in the CNRM model. Therefore, the seasonal change patterns of runoff follow those of precipitation. The results also depended mainly on the global hydrologic model used (GR2M), which was relatively simple and worked with two parameters. Thus, these results can be improved by using a distributed hydrologic model.

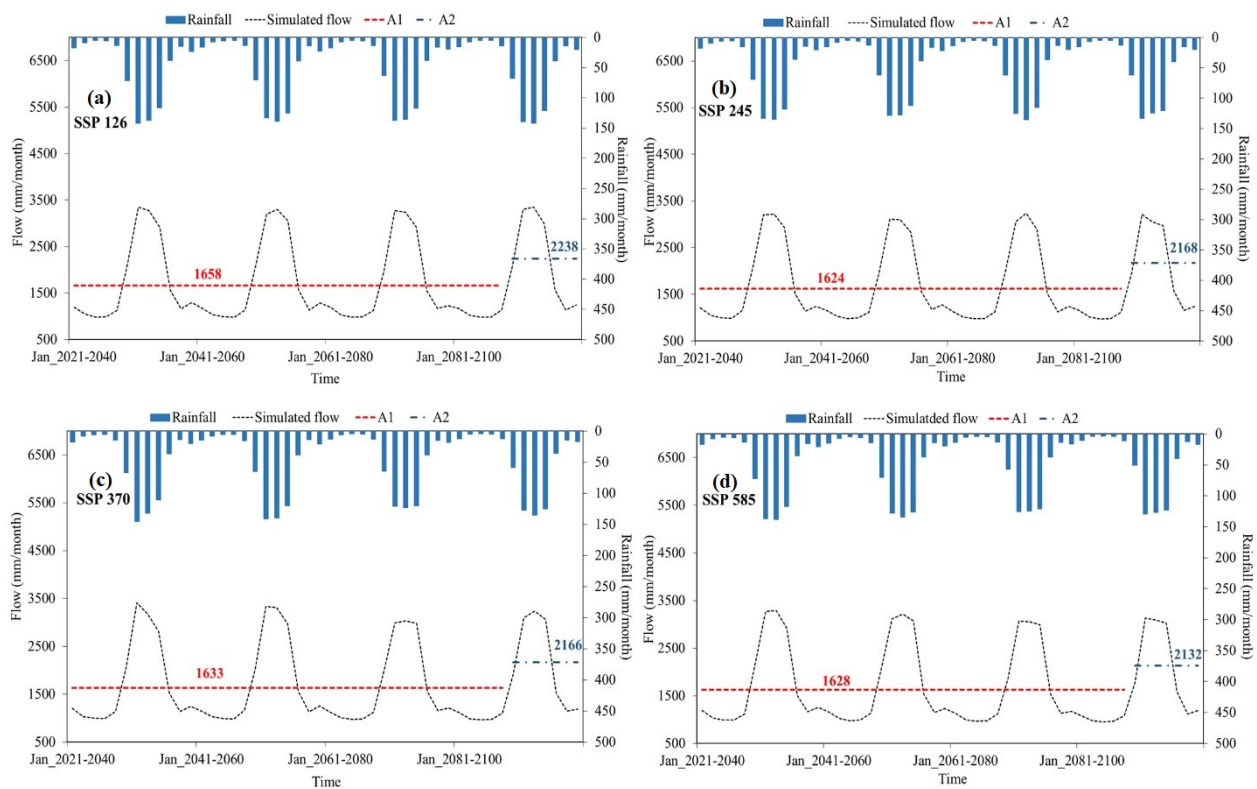


Figure 8. Future flow variation for the analyzed period 2021–2100, under the climate change scenarios (a) SSP 126, (b) 245, (c) 370, and (d) 585. A1 = mean before the break and A2 = mean after the break. The upper bars are the precipitation and the black dashed line is the multidecadal flow for the period 2021–2040, 2041–2060, 2061–2080, and 2081–2100.

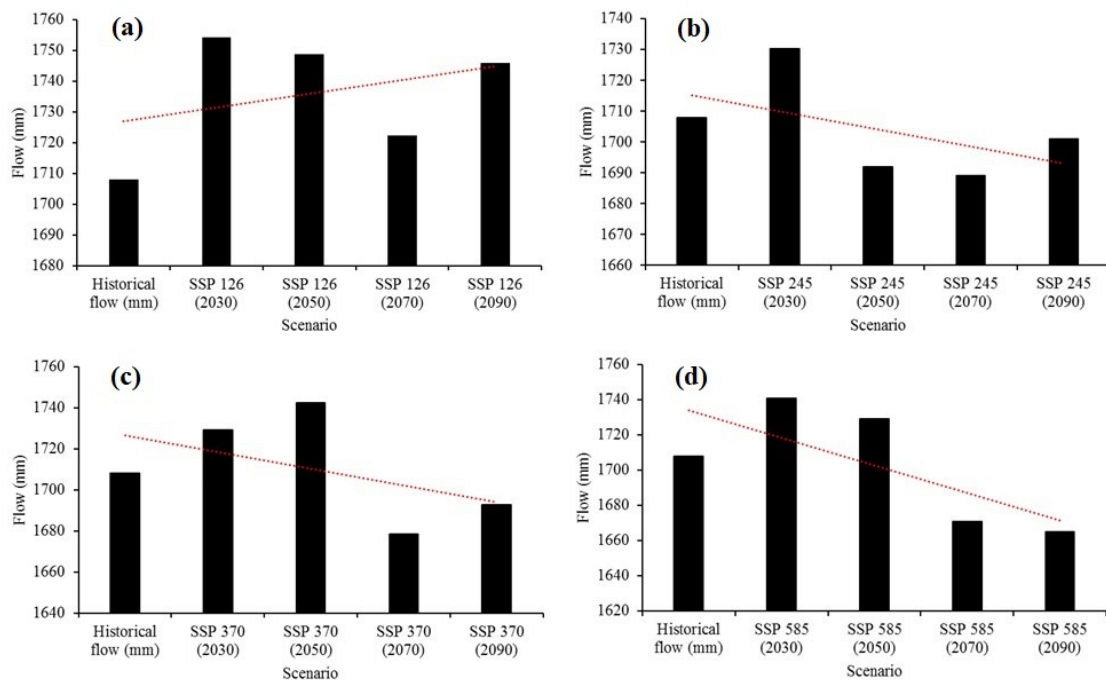


Figure 9. Comparison between the observed average historical flow and the simulated flow under climate change scenarios (a) SSP 126, (b) 245, (c) 370 and (d) 585 in the Sextin River basin. Note: y-axes may be different. The red dotted line is the trend.

The reduction in water resources in important water-producing basins under the effects of climate change has also been modeled for the Conchos River basin in Chihuahua in a study by Rivas and Montero [61,62], where they foresee a reduction in annual runoff of 25%. In the same study, runoff is expected to be reduced by 22% for the Lerma–Chapala basin and 14% for the Grijalva River basin.

As the frequency of droughts increase and surface runoff decreases, the availability of water for the urban and agricultural sectors is expected to decrease. The effect predicted by global circulation models will have a severe impact on agriculture, and adverse repercussions caused by climate change have been seen in the biophysical responses of crops [63]. The increase in temperature causes a decrease in crop productivity due to the reduction in growth periods and the presence of temperatures beyond plants' optimal range of development [64]. Low water availability makes it necessary to implement actions to minimize losses and maximize the efficiency of its use, mainly in the sectors with the highest demand. Given the consequences of climate change on the agricultural sector, actions have focused on reducing irrigation demands by promoting the use of low-water crops that are tolerant to thermal stress, good tillage practices to maintain soil moisture, and encouraging the application of advanced irrigation techniques [65].

Irrigation District 017 has 38,035 thousand users and a surface area of 71,964 ha in the states of Durango and Coahuila, Mexico. The district depends on surface water runoff from the SRB to be used for surface irrigation through canals [66]. Climate change will have an impact on the ecological biodiversity of the SRB, as its resilience capacity will be exceeded by a decrease in surface flows, thus flora and fauna will be significantly affected because many species depend on water runoff from the highlands for their subsistence [67].

In general terms, the four climate change scenarios reflect flow peaks in August. However, in all scenarios, there are significant increases and changes in the seasonal flow cycle (Figure 8), mainly due to changes in the rainfall regime (frequency and intensity) [68]. Although studies have suggested that, the decrease in the intensity of precipitation causes greater impacts on flows compared to frequency [69]. The peak flows may be attributable to the passage of slow-moving baroclinic disturbances, which in turn, could allow for significant precipitation [6]. The reduced flow during April could be attributed to possible low soil moisture caused by the combination of high evaporation rates and low precipitation [6]. Previous studies that have projected small increases in precipitation in this area have not shown significant climate (precipitation and temperature) variability over time [54].

There were limitations to compare observed trends concerning other studies due to the lack of projections with the Coupled Model Intercomparison Projects 6 scenarios for northern Mexico, coupled with the lack of runoff simulation studies under this new generation of scenarios of the Sixth Assessment Report. However, it is possible to make a comparison between equivalent scenarios (e.g., by using the degree of intensity). In flow simulation studies, Cook and Seager [5] and Torres-Alavez et al. [55] found delays in the monsoon period before low carbon dioxide (CO₂) using a representative concentration pathway 2.6, a situation similar to that found in the present study. The trend observed from SSP scenarios 126 to 585 is similar to that found by Chou et al. [70] during the evaluation of climate change with different scenarios for South America using downscaled climate data; however, uniformity between regions is not to be expected, as they may show increases, decreases, or no change [1].

4. Conclusions

Northern Mexico is a region that is currently experiencing changes in climate variability, either due to anthropogenic or natural effects, which cause changes in the hydrological regime of the basins.

Given this climate change, the present research has been developed to evaluate the impact of climate on the hydrology of the SRB, located in northern Mexico, for the period 2021–2100. The PET series for the period 1970–2006 shows an increase of 4.04%. Under climate change scenarios SSP 126, 245, 370, and 585, it shows an increase of 7.64%, 12.12%,

14.15%, and 17.79%, respectively. This information is important because PET is a component of the hydrological cycle, which is linked to the vegetative cover of the region, where high PET rates affect agricultural crops and require a higher demand for water.

The high correlation between precipitation and observed flow from 1970 to 2006 shows a cause–effect phenomenon between both hydrological variables, a situation that often occurs in arid zones. This relationship allows us to analyze the impact on the flow through the amount of precipitation. It is possible to generate more robust linear models if variables, such as atmospheric indices, are included for a more detailed study of flow behavior because this basin is of hydrological importance for Irrigation District 017.

The projected future flow derived from the GR2M model compared to the historical flow observed in the SSP 126 scenario will present an upward trend for the climate horizons in percentages of 2.70%, 2.39%, 0.84%, and 2.22%. SSP 245 shows a downward trend with percentages of 1.30%, −0.94%, −1.10%, and −0.41%. The SSP 370 scenario presents percentages of 1.24%, 2.02%, −1.72%, and −0.88%, respectively, for each climate horizon. Finally, the SSP 585 scenario foresees increases and decreases compared to the observed historical flow of 1.93%, 1.24%, −2.17%, and −2.53%.

The present research is a pioneer in this type of hydrological study for northern Mexico because it uses a more accurate climate change model and the SSP scenarios of CMIP6 of the Sixth Assessment Report, which present improvements compared to their predecessors.

It should be noted that in order to consider the internal variability of global circulation models at smaller scales and lower scenarios, it is important to consider the topographic influence of the study area. Therefore, it implies the use of scenarios with better resolution that reflect a local climate effect. This effect's signal-to-noise ratio could be diluted by using a conglomerate of models while considering those that represent local climate variability.

Author Contributions: Conceptualization, J.E.-Á. and A.R.M.-S.; methodology, J.E.-Á., A.R.M.-S. and V.M.R.-M.; Software, A.R.M.-S.; formal analysis, A.R.M.-S. and J.E.-Á.; investigation, A.R.M.-S. and J.E.-Á.; data curation, A.R.M.-S.; writing—original draft preparation, A.R.M.-S.; writing—review and editing, J.V.-D., V.M.R.-M. and R.T.-C.; supervision, J.E.-Á. All authors have read and agreed to the published version of the manuscript.

Funding: This research received no external funding.

Institutional Review Board Statement: Not applicable.

Informed Consent Statement: Not applicable.

Data Availability Statement: Not applicable.

Conflicts of Interest: The authors declare no conflict of interest.

References

1. Ouhamdouch, S.; Bahir, M.; Ouazar, D.; Goumih, A.; Zouari, K. Assessment the climate change impact on the future evapotranspiration and flows from a semi-arid environment. *Arab. J. Geosci.* **2020**, *13*, 1–14. [CrossRef]
2. Stocker, T.F.; Qin, D.; Plattner, G.K.; Alexander, L.V.; Allen, S.K.; Bindoff, N.L.; Xie, S.P. *Technical Summary: Climate Change 2013. Physical Basis*; Contribution of Working Group I to the Fifth Assessment Report of the Intergovernmental Panel on Climate Change; Cambridge University Press: Cambridge, UK, 2013. Available online: <https://www.ipcc.ch/report/ar5/syr/> (accessed on 1 February 2021).
3. Mokadem, N.; Redhaouia, B.; Besser, H.; Ayadi, Y.; Khelifi, F.; Hamad, A.; Hamed, Y.; Bouri, S. Impact of climate change on groundwater and the extinction of ancient “Foggara” and springs systems in arid lands in North Africa: A case study in Gafsa basin (central of Tunisia). *Euro-Med. J. Environ. Integr.* **2018**, *3*, 28. [CrossRef]
4. Jacoby, G.; Solomina, O.; Frank, D.; Eremenko, N.; D’Arrigo, R. Kunashir (Kuriles) Oak 400-year reconstruction of temperature and relation to the Pacific Decadal Oscillation. *Palaeogeogr. Palaeoclim. Palaeoecol.* **2004**, *209*, 303–311. [CrossRef]
5. Cook, B.; Seager, R. The response of the North American Monsoon to increased greenhouse gas forcing. *J. Geophys. Res. Atmos.* **2013**, *118*, 1690–1699. [CrossRef]
6. Gochis, D.J.; Brito-Castillo, L.; Shuttleworth, W.J. Hydroclimatology of the North American Monsoon region in northwest Mexico. *J. Hydrol.* **2006**, *316*, 53–70. [CrossRef]
7. Sohoulade, D.C.; Singh, V.P. Impact of climate change on the hydrologic cycle and implications for society. *Environ. Soc. Psychol.* **2016**, *1*, 36–49. [CrossRef]

8. Molina-Navarro, E.; Hallack-Alegríab, M.; Martínez-Pérez, S.; Ramírez-Hernández, L.; Mungaray-Moctezuma, A.; Sastre-Merlín, A. Hydrological modeling and climate change impacts in an agricultural semiarid region. Case study: Guadalupe River basin, Mexico. *Agric. Water Manag.* **2015**, *175*, 29–42. [CrossRef]
9. Belarbi, H.; Touaibia, B.; Boumechra, N.; Amiar, S.; Baghli, N. Sécheresse et modification de la relation pluiedébit: Cas du bassin versant de l'Oued Sebdo (Algérie Occidentale). *Hydrol. Sci. J.* **2015**, *62*, 124–136. [CrossRef]
10. Mouelhi, S.; Nemri, S.; Jebari, S.; Slimani, M. Coupling between a Rain-Runoff Model, GR2M, and a Rain Generator to Evaluate the Transfer between Two Dams the Tunisian Semi-Arid Sidi Saad and El Houareb. *Int. J. Innov. Appl. Stud.* **2017**, *19*, 944–959. Available online: <http://www.ijias.issr-journals.org/abstract.php?article=IJIAS-16-140-08> (accessed on 12 February 2021).
11. Segura-Méndez, F.J. Comparative Analysis of Aggregate Water Balance Models in Peninsular Spain and their Sensitivity to Climate Uncertainty. In *Doctoral Program in Urban Planning*; Universidad Católica de Murcia: Murcia, Spain, 2017.
12. Gallo-Llumigusin, K.E.; Iza-Jiménez, B.A. *Modeling with SWAT and GR2M for the Guayllabamba River Sub-Basin, Environmental Engineering Program*; Universidad Técnica de Cotopaxi: Latacunga, Ecuador, 2018.
13. Eyring, V.; Bony, S.; Meehl, G.A.; Senior, C.A.; Stevens, B.; Stouffer, R.J.; Taylor, K.E. Overview of the coupled model Intercomparison project phase 6 (CMIP6) experimental design and organization. *Geosci. Model Dev.* **2016**, *9*, 1937–1958. [CrossRef]
14. Marotzke, J.; Jakob, C.; Bony, S.; Dirmeyer, P.A.; O’Gorman, P.A.; Hawkins, E.; Perkins-Kirkpatrick, E.S.; Le Quéré, C.; Nowicki, S.; Paulavets, K.; et al. Climate research must sharpen its view. *Nat. Clim. Chang.* **2017**, *7*, 89–91. [CrossRef]
15. Nature Climate Change. The CMIP6 landscape. *Nat. Clim. Chang.* **2017**, *9*, 727. [CrossRef]
16. Instituto Nacional de Estadística y Geografía. Mexican Elevation Continuum 3.0, Agusalientes. 2013. Available online: <https://www.inegi.org.mx/app/geo2/elevacionesmex/> (accessed on 17 April 2021).
17. García, E. National Commission for the Knowledge and Use of Biodiversity Climate Koppen Classification, Modified by Garcia. 1998. Available online: <http://www.conabio.gob.mx/informacion/gis/> (accessed on 11 January 2021).
18. Harris, I.; Osborn, T.; Jones, P.; Lister, D. Version 4 of the CRU TS monthly high-resolution gridded multivariate climate dataset. *Sci. Data* **2020**, *7*, 1–18. [CrossRef] [PubMed]
19. Voltaire, A. CNRM-CERFACS CNRM-CM6-1 model output prepared for CMIP6 HighResMIP highres-future. *Earth Sys. Grid Fed.* **2019**. [CrossRef]
20. Makhlof, Z.; Michel, C. A two-parameter monthly water balance model for French watersheds. *J. Hydrol.* **1994**, *162*, 299–318. [CrossRef]
21. Coulibaly, N.; Honoré, T.; Mpakama, Z.; Savané, I. The Impact of Climate Change on Water Resource Availability in a Trans-Boundary Basin in West Africa: The Case of Sassandra. *Hydrology* **2018**, *5*, 12. [CrossRef]
22. Mouelhi, S.; Michel, C.; Perrin, C.; Andréassian, V. Stepwise development of a two-parameter monthly water balance model. *J. Hydrol.* **2006**, *318*, 200–214. [CrossRef]
23. Nash, J.E.; Sutcliffe, J.V. River discharge forecasting through conceptual models. Part I—A discussion of principles. *J. Hydrol.* **1970**, *10*, 282–290. [CrossRef]
24. Moriasi, D.N.; Arnold, J.G.; Van Liew, M.W.; Bingner, R.L.; Harmel, R.D.; Veith, T.L. Model Evaluation Guidelines for Systematic Quantification of Accuracy in Watershed Simulations. *Trans. Am. Soc. Agric. Biol. Eng.* **2007**, *50*, 885–900. Available online: <https://swat.tamu.edu/media/1312/moriasimodeleval.pdf> (accessed on 15 April 2021).
25. Molnar, P. *Calibration. Watershed Modelling, SS 2011*; Institute of Environmental Engineering, Chair of Hydrology and Water Resources management ETH Zürich: Zürich, Switzerland, 2011.
26. Hargreaves, G.H.; Samani, Z.A. Reference crop evapotranspiration from temperature. *Am. Soc. Agric. Eng.* **1985**, *1*, 96–99. [CrossRef]
27. Food and Agriculture Organization. Crop Evapotranspiration, Guidelines for the Determination of Crop Water Requirements. 56 FAO, Irrigation and Drainage Study. 2006. Available online: <http://www.fao.org/3/a-x0490s.pdf> (accessed on 10 January 2021).
28. R Core Team. R: A Language and Environment for Statistical Computing. R Foundation for Statistical Computing, Vienna, Austria. 2020. Available online: <https://www.R-project.org/> (accessed on 5 January 2021).
29. Mann, H.B.; Whitney, D.R. On a Test of Whether One of Two Random Variables is Stochastically Larger than the Other. *Ann. Math. Stat.* **1947**, *18*, 50–60. Available online: <https://www.jstor.org/stable/2236101> (accessed on 14 March 2021). [CrossRef]
30. Pettitt, A.N. A non-parametric approach to the change-point problem. *Appl. Stat.* **1979**, *28*, 126–135. [CrossRef]
31. Mann, H.B. Nonparametric tests against trend. *Econometrica* **1945**, *13*, 245–259. [CrossRef]
32. Kendall, M.G. Multivariate nonparametric tests for trend in water quality. *J. Am. Water Resour. Assoc.* **1988**, *24*, 505–512. [CrossRef]
33. Esquivel-Arriaga, G.; Cerano-Paredes, J.; Sánchez-Cohen, I.; Velásquez-Valle, M.A.; Flores-López, F.; Bueno-Hurtado, P. Temporal analysis of droughts (1922–2016) in the upper Nazas Basin using SPI and its relationships with ENSO. *Tecnol. Cienc. Agua* **2019**, *10*, 126–153. [CrossRef]
34. Cortéz-Villa, J.; Quevedo-Nolasco, A.; Arteaga-Ramírez, R.; Carrillo-Flores, G. Trend of meteorological drought in the state of Durango, Mexico, by the Rodionov method. *Tecnol. Cienc. Agua* **2020**, *11*, 85–131. [CrossRef]
35. Sistemas de Información Geográfica y Medio Ambiente. Atlas de Riesgos Naturales del Municipio de Durango. Prevención de Riesgos en los Asentamientos Humanos [Atlas of Natural Risks in the Municipality of Durango. Risk Prevention in Human Settlements]. Durango. 2013, pp. 1–289. Available online: http://rmgir.proyectomesoamerica.org/PDFMunicipales/2012/10005_Durango.pdf (accessed on 12 January 2021).

36. González-Cervantes, G.; Estrada-Ávalos, J.; González-Barrios, J.L.; Cueto-Wong, J.A.; Sánchez-Cohen, I.; Castillo-Santillán, G. Analysis of Factors Affecting the Rainfall–Runoff Relationship in a Semiarid Zone of Northern Mexico. *Terra Latinoamericana* **2006**, *24*, 337–345. Available online: <https://www.redalyc.org/pdf/573/57311103005.pdf> (accessed on 6 March 2021).
37. Descroix, L.; González-Barrios, J.L.; Vandervaere, J.P.; Viramontes, D.; Bollery, A. An experimental analysis of hydrodynamic behaviour on soils and hill-slopes in a subtropical mountainous environment (Western sierra madre, Mexico). *J. Hydrol.* **2002**, *266*, 1–14. [[CrossRef](#)]
38. Higgins, W.; Douglas, A.; Hahmann, A.; Berbery, E.H.; Gutzler, D.; Shuttleworth, J.; Stensrud, D.; Amador, J.; Carbone, R.; Cortez, M.; et al. Progress in Pan American CLIVAR Research: The North American Monsoon System. *Atmósfera* **2003**, *16*, 29–65. Available online: http://www.scielo.org.mx/scielo.php?script=sci_arttext&pid=S0187-62362003000100003&lng=es&tlng= (accessed on 8 February 2021).
39. Pascale, S.; Carvalho, L.; Adams, D.; Castro, C.; Cavalcanti, I. Current and future variations of the Monsoon of the Americas in warming climate. *Curr. Clim. Chang. Rep.* **2019**, *5*, 125–144. [[CrossRef](#)]
40. Liu, T.; Li, J.; Wang, Q.; Zhao, S. Influence of the autumn SST in the southern Pacific Ocean on Winter precipitation in the North American Monsoon Region. *Atmosphere* **2020**, *11*, 844. [[CrossRef](#)]
41. Intergovernmental Panel on Climate Change (IPCC). Impacts, Adaptation, and Vulnerability. In *Part B: Regional Aspects. Contribution of Working Group II to the Fifth Assessment Report of the Intergovernmental Panel on Climate Change*; Barros, V.R., Field, C.B., Dokken, D.J., Mastrandrea, M.D., Mach, K.J., Bilir, T.E., Chatterjee, M., Ebi, K.L., Estrada, Y.O., Genova, R.C., et al., Eds.; Cambridge University Press: Cambridge, UK; New York, NY, USA, 2014; p. 688. Available online: https://www.ipcc.ch/site/assets/uploads/2018/02/AR5_SYR_FINAL_Front_matters.pdf (accessed on 9 May 2021).
42. Méndez, M.; Magaña, V. Regional aspects of prolonged meteorological droughts over Mexico and Central America. *J. Clim.* **2010**, *23*, 1175–1188. [[CrossRef](#)]
43. Novák, V. Evapotranspiration: A Component of the Water Cycle. In *Evapotranspiration in the Soil-Plant-Atmosphere System*; Springer: Dordrecht, The Netherlands, 2012. [[CrossRef](#)]
44. Sun, S.; Bi, Z.; Zhou, S.; Wang, H.; Li, Q.; Liu, Y.; Wang, G.; Li, S.; Chen, H.; Zhoy, Y. Spatiotemporal shifts in key hydrological variables and dominant factors over China. *Hydrol. Process.* **2021**, *35*, e14319. [[CrossRef](#)]
45. Zhang, S.; Yang, Y.; McVicar, T.R.; Yang, D. An analytical solution for the impact of vegetation changes on hydrological partitioning within the Budyko framework. *Water Resour. Res.* **2018**, *54*, 519–537. [[CrossRef](#)]
46. Zhang, D.; Liu, X.; Zhang, L.; Zhang, Q.; Gan, R.; Li, X. Attribution of evapotranspiration changes in humid regions of China from 1982 to 2016. *J. Geophys. Res. Atmos.* **2020**, *125*, e2020JD032404. [[CrossRef](#)]
47. Cavalcante, B.L.; Pontes, R.M.; Souza, W.M.; de Souza, E.B. Opposite effects of climate and land use changes on the annual water balance in the Amazon arc of deforestation. *Water Resour. Res.* **2019**, *55*, 3092–3106. [[CrossRef](#)]
48. Xie, S.; Mo, X.; Hu, S.; Liu, S. Contributions of climate change, elevated atmospheric CO₂ and human activities to ET and GPP trends in the Three-North Region of China. *Agric. For. Meteorol.* **2020**, *295*, 108183. [[CrossRef](#)]
49. Okkan, U.; Fistikoglu, O. Evaluating climate change effects on runoff by statistical downscaling and hydrological model GR2M. *Theor. Appl. Clim.* **2014**, *117*, 343–361. [[CrossRef](#)]
50. Wang, B.; Jin, C.; Liu, J. Understanding future change of global Monsoons projected by CMIP6 models. *J. Clim.* **2020**, *33*, 6471–6489. [[CrossRef](#)]
51. Higgins, R.W.; Yao, Y.; Wang, X.L. Influence of the North American Monsoon System on the U.S. summer precipitation regime. *J. Clim.* **1997**, *10*, 2600–2622. [[CrossRef](#)]
52. Intergovernmental Panel on Climate Change (IPCC). *Special Report on the Impacts of Global Warming of 1.5 °C Relative to Pre-Industrial Levels and Corresponding Trajectories that Global Greenhouse Gas Emissions Should Follow, in the Context of Strengthening the Global Response to the Threat Climate Change, Sustainable Development and Efforts to Eradicate poverty*. OMM-PNUA; IPCC: Geneva, Switzerland, 2019; p. 32. Available online: https://www.ipcc.ch/site/assets/uploads/sites/2/2019/09/SR15_Summary_Volume_spanish.pdf (accessed on 6 April 2021).
53. Intergovernmental Panel on Climate Change (IPCC). Climate Change 2007. Synthesis Report. Contribution of Working Groups I, II and III to the Fourth Assessment Report of the Intergovernmental Panel on Climate Change. Suiza. 2007. Available online: <https://www.ipcc.ch/languages-2/spanish/ipcc-en-espanol-publications/> (accessed on 10 March 2021).
54. Cavazos, T.; de Grau, P.; Martínez, A.; Conde, C.; López, L.; Nava, S. Study for the Incorporation of New Variables in the Climate Change Scenarios for Mexico used in the Fifth National Communication. 2014. Available online: <https://www.gob.mx/inecc/documentos/adaptacion-al-cambio-climatico> (accessed on 14 March 2021).
55. Torres-Alavez, A.; Cavazos, T.; Turrent, C. Land–Sea Thermal Contrast and Intensity of the North American Monsoon under Climate Change Conditions. *J. Clim.* **2014**, *27*, 4566–4580. [[CrossRef](#)]
56. Baek, H.J.; Lee, J.; Lee, H.S.; Hyun, Y.K.; Cho, C.; Kwon, W.T.; Marzin, C.; Gan, S.Y.; Kim, M.J.; Choi, D.H.; et al. Climate Change in the 21st Century Simulated by HadGEM2-AO under Representative Concentration Pathways. *Asia-Pacific J. Atmos. Sci.* **2013**, *49*, 603–618. [[CrossRef](#)]
57. Ouhamdouch, S.; Bahir, M. Climate change impact on future rainfall and temperature in semi-arid areas (Essaouira Basin, Morocco). *Environ. Process.* **2017**, *4*, 975–990. [[CrossRef](#)]

58. Jung, M.; Reichstein, M.; Ciais, P.; Seneviratne, S.I.; Sheffield, J.; Goulden, M.L.; Bonan, G.; Cescatti, A.; Chen, J.; de Jeu, R.; et al. Recent decline in the global land evapotranspiration trend due to limited moisture supply. *Nature* **2010**, *467*, 951–954. [[CrossRef](#)] [[PubMed](#)]
59. Miralles, D.G.; Van den Berg, M.; Gash, J.H.; Parinussa, R.M.; de Jeu, R.; Beck, H.E.; Holmes, T.; Jiménez, C.; Verhoest, N.; Dorigo, W.A.; et al. El Niño-La Niña cycle and recent trends in continental evaporation. *Nat. Clim. Chang.* **2013**, *4*, 122–126. [[CrossRef](#)]
60. Yao, Y.; Qu, W.; Lu, J.; Cheng, H.; Pang, Z.; Lei, T.; Tan, Y. Responses of Hydrological Processes under Different Shared Socioeconomic Pathway Scenarios in the Huaihe River Basin, China. *Water* **2021**, *13*, 1053. [[CrossRef](#)]
61. Rivas, I.; Montero, M. Downscaling Technique to Estimate Hydrologic Vulnerability to Climate Change: An Application to the Conchos River Basin, Mexico. *J. Water Clim. Chan.* **2013**, *4*, 440–457. [[CrossRef](#)]
62. Rivas, I.; Montero, M. Assessment of Surface Runoff Vulnerability to Climate Change of the Lerma-Chapala Basin, Mexico. *J. Water Resour. Plan. Manag.* **2014**, *140*, 04014042. [[CrossRef](#)]
63. Ojeda, W.; Martínez, P.; Hernández, L. Repercussions of Climate Change on Irrigated Agriculture. In *Effects of Climate Change on Mexico's Water Resources*; Martínez, P., Aguilar, A., Eds.; Mexican Institute of Water Technology: Morelos, Mexico, 2008; Volume 2, pp. 73–83. Available online: https://www.researchgate.net/publication/291164839_Effects_of_climate_change_on_Mexicos_water_resources (accessed on 11 March 2021).
64. Gadgil, D. Climate Change and Agriculture: An Indian perspective. *Curr. Sci.* **1995**, *9*, 649–659. Available online: <https://www.jstor.org/stable/24097258> (accessed on 12 December 2021).
65. Rivas-Acosta, I. *Effects of Climate Change on Mexico's Water Resources (Surface Water)*; Mexican Institute of Water Technology: Morelos, Mexico, 2015; ISBN 978-607-9368-09-8. Available online: <http://repositorio.imta.mx/handle/20.500.12013/1601> (accessed on 10 January 2021).
66. Sistema Nacional de Información del Agua. Irrigation Districts. National Water Information System. National Water Commission. 2019. Available online: <http://sina.conagua.gob.mx/sina/index.php> (accessed on 17 May 2021).
67. Food and Agriculture Organization. Consequences of Climate Change. 2013. Available online: <http://www.fao.org/3/i2498s/i2498s04.pdf> (accessed on 5 February 2021).
68. Hsu, K.C.; Li, S.T. Clustering spatial-temporal precipitation data using wavelet transform and self-organizing map neural network. *Adv. Water Resour.* **2010**, *33*, 190–200. [[CrossRef](#)]
69. Boubacar, I.; Karambiri, H.; Polcher, J. Hydrological Impacts of the Changes in Simulated Rainfall Fields on Nakanbe Basin in Burkina Faso. *Climate* **2015**, *3*, 442–458. [[CrossRef](#)]
70. Chou, S.C.; Lyra, A.; Mourão, C.; Dereczynski, C.; Pilotto, I.; Gomes, J.; Bustamante, J.; Tavares, P.; Silva, A.; Rodríguez, D.; et al. Assessment of Climate Change over South America under RCP 4.5 and 8.5 Downscaling Scenarios. *Am. J. Clim. Chang.* **2014**, *3*, 512–527. [[CrossRef](#)]

Disclaimer/Publisher's Note: The statements, opinions and data contained in all publications are solely those of the individual author(s) and contributor(s) and not of MDPI and/or the editor(s). MDPI and/or the editor(s) disclaim responsibility for any injury to people or property resulting from any ideas, methods, instructions or products referred to in the content.